Molecular dynamics simulation of thermal de-icing on a flat surface

Qiangqiang Sun[a], Yong Zhao[b], Kwing-So Choi[a], Xuerui Mao[a,*]

[a] *Faculty of Engineering, University of Nottingham, Nottingham, NG7 2RD, UK.*
[b] *AVIC Aerospace Systems, Chaoyang District, Beijing, 100028, China.*

Abstract

The accumulation of ice has adverse effects on human activities but the dynamic mechanism of icing and de-icing has not been well clarified. Herein, molecular dynamics (MD) simulations and the analysis methods of the hydrogen bond and the tetrahedral order parameter are used for the first time to investigate the underpinning physics and visualize the thermal de-icing process on a flat wall from the molecular level. The effects of ice thickness (H), wall temperature (T_w) and wettability on the thermal de-icing process are examined. The results indicate that the ice starts to melt from its mantle and then proceeds inwards. The energy consumption of thermal de-icing can be modelled as a bilinear function of T_w and H. The melting time is almost bilinear with respect to H and $1/(T_w - 273.15\,K)$, and converges to a constant value at $T_w \geq 313.15\,K$. When adopting a hydrophobic surface, which is generally considered as icephobic and prevents the ice accretion, more time and almost constant energy are required to melt the ice. By revealing thermal de-icing processes on a hot surface at the molecule level, this work offers guidance for the development of de-icing techniques and devices applied extensively in engineering applications.

Keywords:
Molecular dynamics simulation, Thermal de-icing, Hexagonal ice, Hydrogen bond, Tetrahedral order parameter

1. Introduction

De-icing has been of great interest because the excessive accumulation of ice can cause devastating effects. According to statistics, around 30% of the traffic accidents in the winter have resulted from the accumulation of ice on the railroad and bridge surfaces, and the corresponding economic loss can reach up to hundreds of millions of dollars per day [1, 2]. Also, due to the low atmospheric temperature ranging from -40 ℃ to 0 ℃, the icing phenomenon appears

*Corresponding author
Email address: Xuerui.Mao@nottingham.ac.uk (Xuerui Mao)

Nomenclature:

E	energy, eV	**Greek symbols**	
H	thickness of ice layer, Å	ϵ	well-depth of the Lennard-Jones potential, eV
i, j, k	atom index	ϵ_{HH}	well-depth between two H atoms, eV
m_H	mass of H atom, g/mol	ϵ_{OH}	well-depth between O and H atom, eV
m_O	mass of O atom, g/mol	ϵ_{OO}	well-depth between two O atoms, eV
N	total number of atoms	ϵ_{Ag-Ag}	well-depth between two silver atoms, eV
q_H	charge of H atom, g/mol	ϵ_{Ag-O}	well-depth between silver and O atom, eV
q_O	charge of O atom, g/mol	ρ	density, g/cm^3
Q	tetrahedral order parameter	σ	collision diameter, Å
r	distance between two atoms, Å	σ_{HH}	collision diameter between two H atoms, Å
r_{cc}	cutoff distance for Coulomb force, Å	σ_{OH}	collision diameter between O and H atom, Å
r_{hb}	cutoff distance of hydrogen bond, Å	σ_{OO}	collision diameter between two O atoms, Å
r_0	distance between O and H atom in a water molecule, Å	σ_{Ag-Ag}	collision diameter between two Ag atoms, Å
r_{OM}	distance between the O atom and additional site, Å	σ_{Ag-O}	collision diameter between silver and O atom, Å
t	time, ns	θ	angle between water molecules , °
T	temperature, K	θ_0	angle of a water molecule, °
T_w	wall temperature, K	θ_{hb}	cutoff angle, °
y	cartesian coordinate, Å	**Superscript**	
U	potential energy, eV	$*$	dimensionless quantity

frequently at the leading edges of wings (see Fig. 1), rotor blades and propellers when the water drops in clouds impinge on the aircraft [3, 4]. The ice accretion can dramatically reduce the engine and propellers' efficiency, and affect the moment characteristics of the aircraft (i.e., decreasing the lift and increasing the drag force) [5]. These effects then pose a serious threat to flight safety and may lead to flight catastrophes. Therefore, over the last several decades, a variety of passive and active de-icing and anti-icing methods have been explored. Compared with the active ice removal approaches, the passive methods including fabricating various anti-icing coatings and modifying wall surface topography, etc. were complex and difficult to apply widely although they do not require external energy inputs [6]. Most importantly, the passive methods do not work solely and have to be applied with active approaches for safety concerns. One popular active approach was to exploit the chemical reactions by e.g. adding salt to the ice, and so far over 30 million tons of salt has been employed, leading to environmental pollution and damage [7]. Most importantly, the ice could not be melted by the salt when the temperature was below -3.9 ℃ [8].

As an alternative, the environmentally-friendly thermal ice removal technique has been also actively discussed. At the macroscale, Mauro et al. [2] tested to use the geothermal energy to melt the ice by inserting a high thermal conductivity material (e.g., aluminum) in the ground as a pathway for the spontaneous transfer of the geothermal energy to the street surface. Li et al. [9] designed a self-de-icing road system via combining the carbon nano-fiber polymer thermal source and some high thermal conductive composites, and performed experiments on

the melting time and energy consumption. Liu et al. [10] proposed the design and operation parameters for the electric heating pipes employed to melt ice on the pavement. Liu et al. [11] conducted a theoretical analysis and experimental investigation on the heat transfer process of ice accreting on the airfoil surface. They concluded that the convective heat transfer process could be enhanced by the ice accreting near the leading edge of aircraft wings, and the ice accumulation could also be further promoted by the enhanced convective heat transfer. Karim et al. [12] produced the graphene-coated glass roving that has low energy cost and high thermal conductivity, and could be used in various thermal de-icing applications.

As mentioned above, the thermal de-icing issue has been widely investigated in numerical simulations and experiments from the macro level. However, many details on the thermal de-icing and the ice/water equilibrium were very difficult to observe and clarify by those efforts [13]. The molecular dynamics (MD) simulation was a powerful approach to investigate the ice bulk melting, and it could reveal the underlying physical mechanisms (i.e., the transition to the disordered state) [14]. Also, the size effects of the computational domain could be eliminated by the periodic boundary conditions used in MD simulations [15, 16]. For example, Mochizuki et al. [14] explored the defects of the hydrogen bonds, and concluded that the defect pair separation was the controlling step when ice was heated to melt. A quasi-liquid layer was observed at the interface between the ice and SiO_2 below the bulk melting temperature by Engemann et al. [17], and the same conclusion was reported by Sanchez et al. [18]. The entropic analysis of phase transitions was applied to analyze the physical details such as latent heats, equilibrium transition temperatures and surface tensions, and a function between the statistical temperature and enthalpy was obtained [19]. Pan et al. [20] employed the MD simulation to study the melting, and observed that the melting temperature strongly depends on the size of ice. Similarly, the effects of ice cluster size on the melting point were explored by Egorov et al. [21], and a nonmonotonic decrease in melting temperature was observed for smaller clusters. Despite the recent progress, there are several interesting and vital issues that have still not been tackled: (1) although the thermal de-icing was extensively studied in previous macroscale experiments, there are no approximation equations for the melting time and energy consumption, and the snapshots recorded by the camera cannot accurately show the interface between the ice and water during the melting process. Meanwhile, previous MD simulations mainly focused on the underlying physical mechanism (i.e., the defects of the hydrogen bonds network, the quasi-liquid water layer at the ice-wall interface and the reduction of the melting temperature) rather than the melting time and energy cost primarily considered in engineering applications; (2) the effects of the wall wettability on the melting have rarely been investigated

thoroughly. To address these points, MD simulations will be deployed in this work, along with the analysis of the hydrogen bond and the tetrahedral order parameter.

A critical challenge to apply the MD simulations to investigate the thermal de-icing process is the criterion to distinguish water and ice molecules. Mochizuki et al. [14] identified the water

Figure 1: Ice accumulation on the wing of an aircraft. Adapted and reprinted with permission from reference [22].

molecules from the ice structure through evaluating if the molecule is "off-lattice". Namely, an ice molecule was considered to become water if the distance between the particle and the nearest lattice point of the ice crystal with regular shape is more than 1 Å. Moore et al. [23] introduced the CHILL algorithm based on the local bond order parameter method [24]. The coherence of molecules' orientational order with that of their neighbours was employed to distinguish whether they belong to the crystal or liquid phase. Errington et al. [25] proposed the tetrahedral order parameter which was extensively applied to define ice-like and liquid-like molecules [20, 26–29], and the parameter was computed as

$$Q_i = 1 - \frac{3}{8}\sum_{j=1}^{3}\sum_{k=j+1}^{4}\left(\cos\theta_{\mathrm{j,i,k}} + \frac{1}{3}\right)^2, \tag{1}$$

where i, j and k are indices for O atoms. The angle $\theta_{j,i,k}$ is formed by the O atoms of j, i and k (i is the vertex of the angle). Following Conde et al. [26], a molecule was classified as ice-like when $0.91 \leq Q_i \leq 1$. Also, the averaged hydrogen bonds for ice or water molecules are different. For example, the averaged hydrogen bonds for water molecules at 25 ℃ or ice molecules were estimated as 3.59 or 4.0, respectively [30]. Therefore, the time averaged value of the number of hydrogen bonds for each ice/water molecule was argued by Carignano et al. [31] as a reasonable physical quantity to identify the ice or water molecules. Although there are many definitions of the hydrogen bond such as the energetic definition through computing the potential energy of each pair of ice/water molecules [32], the electronic structure-based method and the geometric

distance-angle definition [33], the geometric distance-angle identification criterion is used for simplicity. In this method, two parameters, the cutoff angle (θ_{hb}) between the OH hydrogen bond and the OH covalent bond, and the cutoff distance (r_{hb}) between the O and H atoms at different molecules, should be defined appropriately. If the distance (r) between the H and O atoms on different molecules and the angle (θ) between water molecules meet the condition: $r \leq r_{hb}$ and $\theta \leq \theta_{hb}$, a hydrogen bond is considered to be existing. Similar to reference [13], r_{hb} and θ_{hb} are chosen as 3.5 Å and 40 °, respectively. In this work, both the averaged tetrahedral order parameter and hydrogen bonds for each ice/water molecule are applied to identify the water molecules from the ice.

The main results of this study include (1) the melting time is almost a linear function with respect to H and $1/(T_w - 273.15)$, and the energy cost can be evaluated as a linear function of the wall temperature with the slope increasing with the ice thickness; (2) the melting process is well visualized and the time evolution of the interface between the ice and quasi-liquid layer is obtained; (3) a strong wettability dependence of the melting time is observed while the energy cost is almost independent of the wall wettability. The rest of this paper is outlined as follows: the methodology and details of simulation systems are described in Section 2. The effects of the wall temperature, thickness of ice layer and wall wettability on the melting time and energy cost are presented in Section 3, and then the thermal de-icing process is visualized through analyzing the average hydrogen bonds and tetrahedral order parameter in Section 4. Finally, conclusions are drawn in Section 5.

2. Details of MD simulations

As depicted in Fig. 2a, hexagonal ice molecules (ice I_h) are investigated in this work because of their ubiquity in nature (see Appendix A for the generation of ice I_h structure). For the silver wall whose cross-sectional area is 95×95 Å^2, it is simulated with a face-centered cubic unit with a lattice constant of 4 Å. The wall model and Langevin thermostat [34] are employed to introduce physically-sound heat flux through the silver wall. Namely, the silver wall is divided into three sections. The bottom silver atoms marked in blue in Fig. 2b and Fig. 2c are fixed to prevent atoms from penetration, the red silver atoms are controlled by the aforementioned Langevin thermostat method to the prescribed temperature and the cyan particles are "real" silver atoms that can vibrate freely. In total, there are 17150 atoms for the wall and $13104 - 137592$ molecules of ice (at thickness $H = 40 - 160$ Å) considered in the simulation.

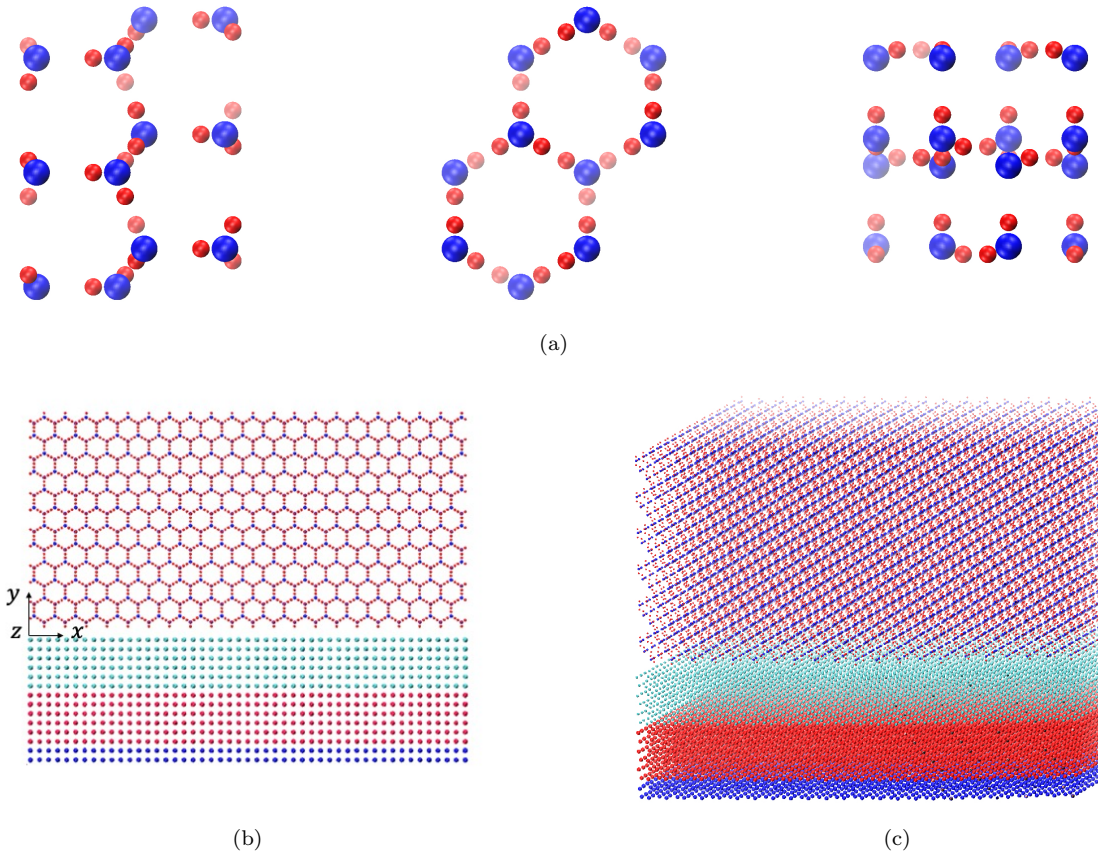

(a)

(b)

(c)

Figure 2: Sketch of the MD simulation system. (a) Ice I_h model from the side, front and top views. (b) and (c) show the ice-silver system from two-dimensional and three-dimensional views, respectively, and the cyan, red and blue particles below the ice are the three layers of silver atoms.

The freezing temperature of water predicted by the well-known SPC/E or TIP4P model is $215\,K$ or $232\,K$, respectively [35]. The four-site water model (TIP4P/ice) [35] describes more accurately the near freezing point and bulk properties of the ice and water (see Table 1 for all parameters). For example, it predicts that the water freezing point is $272.2\,K$, very closer to the value of $273.15\,K$ observed in experiments. Therefore, TIP4P/ice model is applied to model the ice and water in this work. A large time step of $1.0\,fs$ in all simulation cases is enabled by adopting the SHAKE algorithm to constrain the bonds and angles of ice/water molecules, and the long-range electrostatic interactions are solved by employing the PPPM method [36].

The interactions of silver atoms are described by the 12-6 Lennard-Jones (LJ) pair-wise potential proposed by Jones et al. [37]:

$$U(r) = 4\epsilon \left[\left(\frac{\sigma}{r}\right)^{12} - \left(\frac{\sigma}{r}\right)^{6} \right], \tag{2}$$

where ϵ is the well-depth of the Lennard-Jones potential and σ is the collision diameter. $\epsilon_{Ag-Ag} = 0.4080\,eV$ and $\sigma_{Ag-Ag} = 2.551$Å, respectively [38]. Moreover, only the interactions between the silver and oxygen atoms in ice/water molecules are calculated, and the LJ poten-

Table 1: Parameters for the TIP4P/ice potential.

Parameter	Values	Unit
m_H	1.008	g/mol
m_O	15.9994	g/mol
q_H	0.5897	e
q_O	-1.1794	e
r_0	0.9572	Å
θ_0	104.52	°
r_{OM}	0.1577	Å
ϵ_{OO}	9.1427×10^{-3}	eV
σ_{OO}	3.1668	Å
ϵ_{HH}	0	eV
σ_{HH}	0	Å
ϵ_{OH}	0	eV
σ_{OH}	0	Å
r_{cc}	8.5	Å

tial is also used to compute the atomistic forces. ϵ_{Ag-O} and σ_{Ag-O} are determined from the Lorenz-Bertholot rule [39, 40]:

$$\varepsilon_{Ag-O} = \sqrt{\varepsilon_{Ag-Ag}\,\varepsilon_{O-O}} = 0.0611\,eV\,, \tag{3a}$$

$$\sigma_{Ag-O} = \frac{\sigma_{Ag-Ag} + \sigma_{O-O}}{2} = 2.8589\,\text{Å}\,. \tag{3b}$$

The Large-scale Atomic/Molecular Massively Parallel Simulator (LAMMPS) package is used to perform all simulations. The periodic boundary conditions in all three directions are used throughout the work. It should be pointed out that a vacuum space with the same thickness from the top of the ice to the bottom of the silver substrate is added to the top of the ice to eliminate the interaction between the top ice atoms and the bottom substrate atoms resulting from the periodic boundary condition. Each case includes the following three steps: (1) similar to reference [13], the temperature of the ice-silver system is adjusted to $260\,K$ through the Langevin thermostat approach for $0.4\,ns$ under the NVT ensemble to ensure that the equilibration state is achieved; (2) silver atoms shown in red are then heated to a given temperature while maintaining the ice temperature at $260\,K$ through applying the Langevin thermostat (wall atoms marked in cyan oscillate freely) and (3) the thermostat algorithm is then removed from ice molecules to melt the ice by the hot wall.

To validate the accuracy of this work, the average number of hydrogen bonds and tetrahedral order parameters ($< Q >= (1/N)\sum_i^N Q_i$, where N is the total number of O atoms [27]) for each ice/water molecule are computed by our Tool Command Language (TCL) script, and the results are summarized in Table 2. One can observe that the maximum relative error between

Table 2: The average number of hydrogen bonds and tetrahedral order parameters $< Q >$ for each ice/water molecule at various temperature.

			reference value	present work	relative error
Hydrogen bonds	ice		4 [30]	3.99	0.25%
	water	273.15 K	3.69	3.77	2.17%
		298.15 K	3.59	3.66	1.95%
		333.15 K	3.41	3.51	2.93%
		373.15 K	3.24	3.33	2.78%
$< Q >$	ice		1 [25]	0.95	5.00%
	water	295 K	0.70 [28] or 0.678 [29]	0.69	1.43% or 1.77%

our results and the reference is less than 5%. The result also validates the TCL code that will be used to visualize the thermal de-icing process in Section 4.

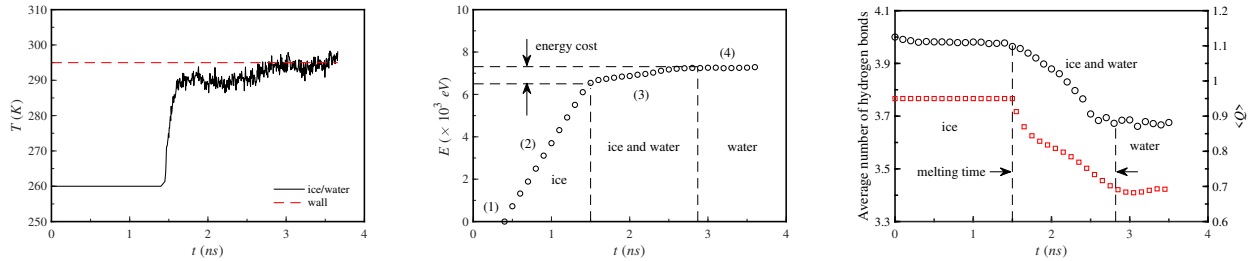

(a) (b) (c)

Figure 3: (a) Temperature (T), (b) energy input (E) and (c) the average number of hydrogen bonds and the tetrahedral order parameter per ice/water molecule during the thermal de-icing process at $T_w = 295\,K$, $H = 40$ Å, $\epsilon_{Ag-O} = 0.0611eV$ and $\sigma_{Ag-O} = 2.8589$ Å, respectively.

3. Effects of wall temperature and wettability on thermal de-icing

The thermal de-icing on the silver surface is studied by following the three MD simulation steps illustrated in Section 2. As shown in Fig. 3a, the initial temperature of the ice and silver wall is artificially modulated to 260 K and 295 K, respectively, via the Langevin thermostat. Within a very short time after the thermal de-icing process starts, the ice/water temperature jumps to around 290 K, and then increases mildly to the wall temperature. One should note that the oscillation of ice/water temperature as seen in Fig. 3a is caused by the thermal fluctuations of ice/water molecules.

The cumulative energy input applied to heat the wall is displayed in Fig. 3b, which is a constant value at the equilibrium state or the state where all ice molecules are melted. This validates the rationality of the simulation setup. The energy cost at stage (2) is used to heat "real" silver atoms before melting ice. The energy consumption during the thermal de-icing

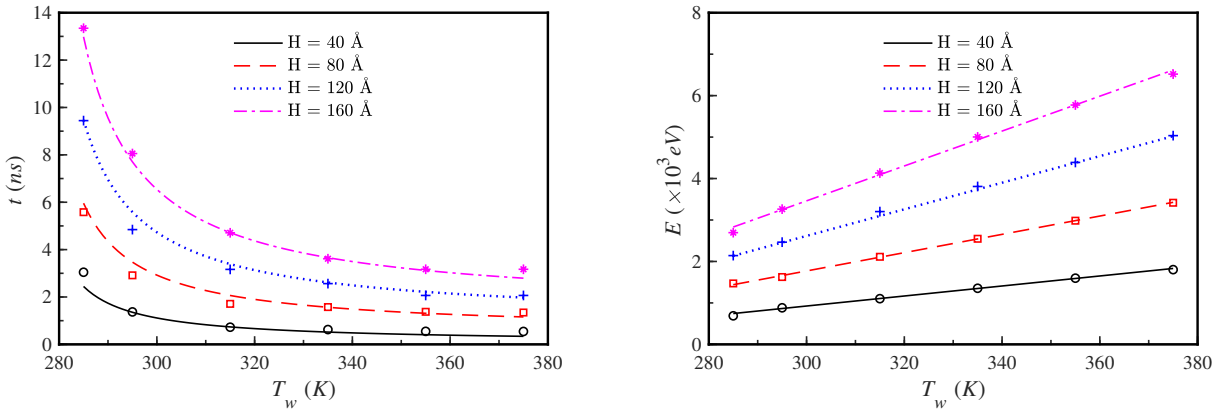

(a) (b)

Figure 4: (a) De-icing time and (b) energy cost at various thickness and wall temperature with $\epsilon_{Ag-O} = 0.0611\,eV$ and $\sigma_{Ag-O} = 2.8589\,\text{Å}$. Curves and scatter points are computed from fitting equations shown in Eq. (4) and simulation results, respectively.

process is then defined as the difference of the cumulative energy at stages (2) and (4). With the melting of ice, the number of averaged hydrogen bonds and the tetrahedral order parameter shown in Fig. 3c decrease gradually in good agreement, and the time consumption is then defined as the melting time.

Comparing Fig. 3a and Fig. 3c, the averaged number of hydrogen bonds for each water/ice molecule is found to be around 4.0 at the time when the ice temperature increases suddenly. This indicates that the thermal melting process can be roughly divided into two stages: ice temperature rises rapidly to the wall temperature, and then ice starts to melt gradually. Further details on the melting snapshots will be clarified later.

The thermal de-icing at various thickness and wall temperature is then investigated, and the result is shown in Fig. 4. At a higher temperature, for example, $T_w = 375\,K$, the ice I_h crystal collapses as soon as it is heated. The fast thermal de-icing process for the case of high wall temperature is in agreement with previous observation [14]. Besides, the melting time decreases sharply to almost a constant value at $T_w \geq 313.15\,K$ while the corresponding energy cost almost increases linearly. Hence, it is unnecessary to adopt higher wall temperatures during the practical design and applications, as also reported in reference [41]. The thermal de-icing time and energy consumption shown in Fig. 4 can be approximated by the following equations with a root mean square error less than 1%:

$$t\,(T_w, H) = \frac{0.9033H - 7.903}{T_w - 273.15} + 0.01158H - 0.4005\,, \tag{4a}$$

$$E(T_w, H) = (0.25H + 2.078)T_w - 53.86H - 543.9\,, \tag{4b}$$

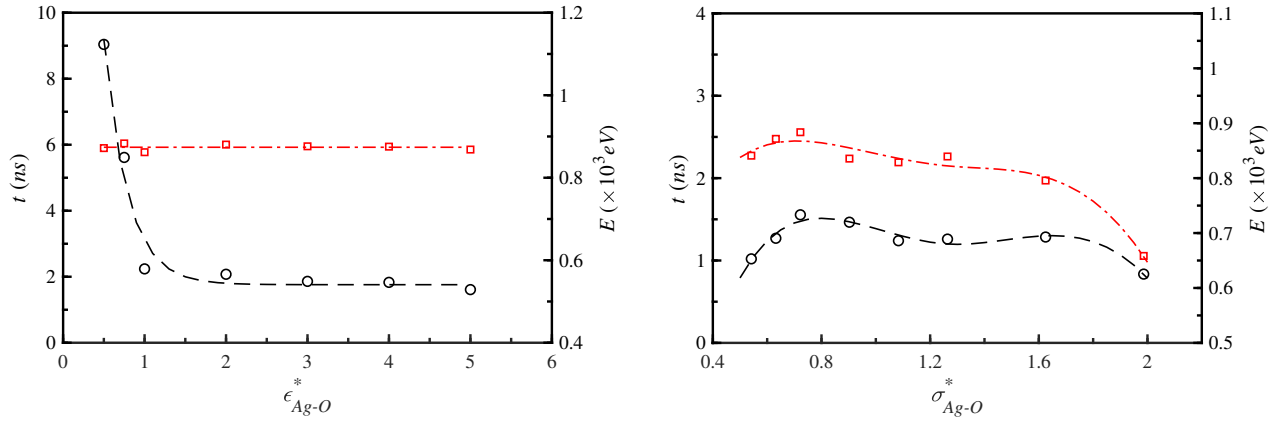

(a) (b)

Figure 5: Energy cost and de-icing time at various ϵ^*_{Ag-O} and σ^*_{Ag-O}. (a) $\sigma_{Ag-O} = 2.8589\,\text{Å}$, $H = 40$ Å and $T_w = 295\,K$. (b) $\epsilon_{Ag-O} = 0.0611\,eV$, $H = 40$ Å and $T_w = 295\,K$. Red dash-dotted line and black dash line represent the energy cost and melting time, respectively. Curves and scatter points are fitting and simulation results, respectively.

where the units for t, T_w, H and E are ns, K, Å and eV, respectively. These formulas suggest that the melting time is a bilinear function of H and $1/(T_w - 273.15\,K)$ while the energy consumption is bilinear to H and T_w.

According to previous efforts, the wettability of a solid wall is also an important factor affecting the accumulation of ice. Therefore, we change the interaction strength ($\epsilon^*_{Ag-O} = \epsilon_{Ag-O}/\epsilon_{O-O}$, a larger ϵ^*_{Ag-O} means a hydrophilic wall surface) while fixing the wall temperature as $295\,K$ to examine the effects of this parameter on thermal de-icing, and the result is shown in Fig. 5a. The energy consumption is almost independent of wall wettability. The melting time reduces at a larger ϵ^*_{Ag-O}, and can be approximated as

$$t\left(\epsilon^*_{Ag-O}\right) = 7.48exp\left(-3.435\epsilon^*_{Ag-O} + 1.711\right) + 1.759. \tag{5}$$

This observation indicates that more time is required to melt the ice accreted on the hydrophobic surface although such a surface is generally considered as the anti-icing material [42, 43]. Similarly, the collision diameter ($\sigma^*_{Ag-O} = \sigma_{Ag-O}/\sigma_{O-O}$) is also varied, and the corresponding melting time and energy consumption increase firstly and then decrease (see Fig. 5b).

4. Physics of the thermal de-icing

In Section 3, we have illustrated the effects of wall temperature and wettability and the thickness of ice on the thermal de-icing time and energy consumption. The physical details during the process of thermal de-icing will be examined in this section.

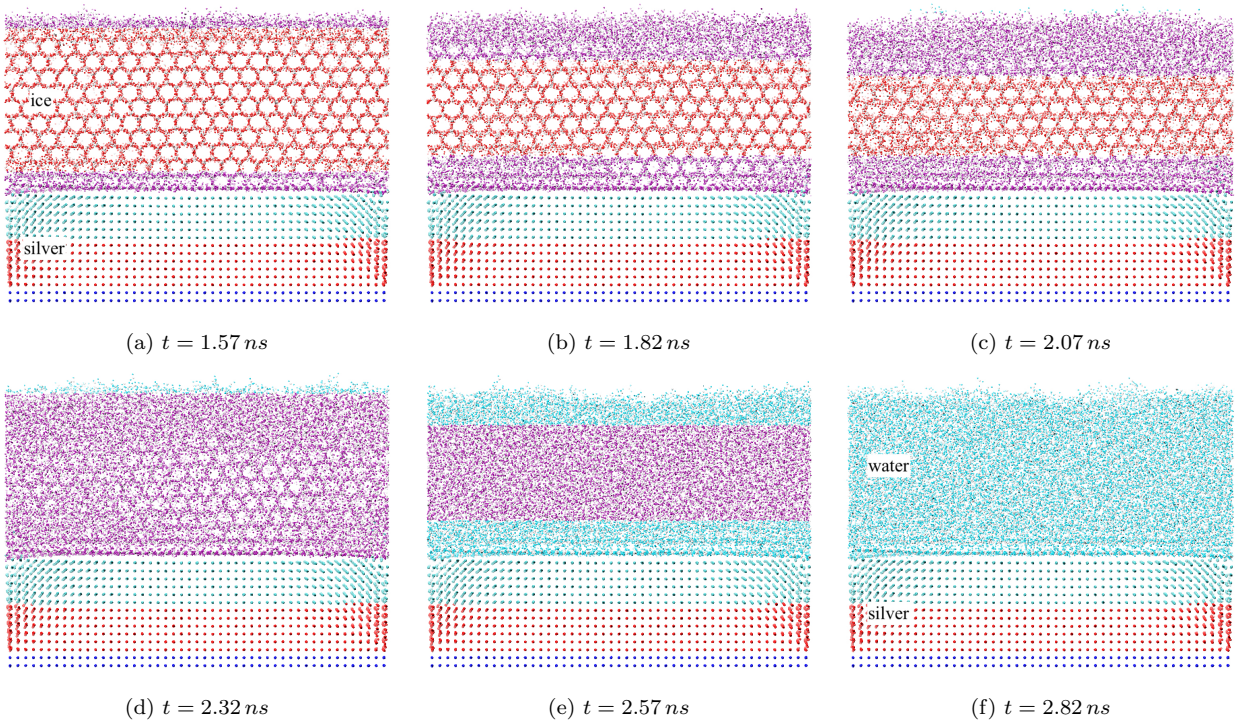

(a) $t = 1.57\,ns$ (b) $t = 1.82\,ns$ (c) $t = 2.07\,ns$

(d) $t = 2.32\,ns$ (e) $t = 2.57\,ns$ (f) $t = 2.82\,ns$

Figure 6: Snapshots of thermal de-icing at $T_w = 295\,K$, $H = 40$ Å, $\epsilon_{Ag-O} = 0.0611\,eV$ and $\sigma_{Ag-O} = 2.8589$ Å. The shallow blue or red particles denote the water or ice molecules, respectively, and the purple one is the phase between ice and water.

Here, the case with $T_w = 295\,K$, $H = 40$ Å and $\epsilon_{Ag-O} = 0.0611\,eV$ and $\sigma_{Ag-O} = 2.8589$ Å is considered as an example to show the thermal de-icing process (the de-icing processes at other combinations of parameters are similar, and are not presented for brevity). The ice structure is divided into 10 bins with a height of 4 Å along the wall-normal direction. The averaged number of hydrogen bonds for each ice/water molecule is then computed by the aforementioned TCL script for each bin at a prescribed time step. Based on this method, the melting snapshots are then displayed in Fig. 6. One can observe that there is a quasi-liquid layer between the ice and the silver wall at the beginning of the thermal de-icing process, and this observation coincides with previous efforts [17, 18]. Besides, an interesting observation is that the ice begins to melt from the top and the bottom surfaces, and proceeds inwards, as shown in Fig. 7. This is in agreement with the previous experiment [7] and simulation where the local bond order parameter method introduced in Section 1 was employed to distinguish ice and water molecules [18, 44, 45].

It is worth noting that this thermal de-icing process is not caused by the periodic boundary conditions imposed in the simulations. To validate, the temperature distributions for four bins are sampled. If the outer-to-center thermal de-icing process is caused by the simulation setup of periodic boundary conditions, the temperature of the top and bottom ice bin should be equal

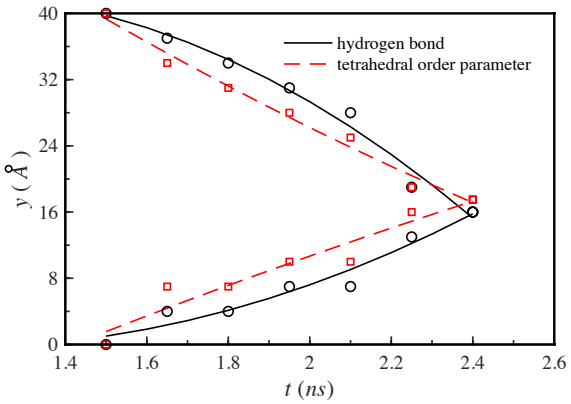

Figure 7: The profile of the melting front location (namely, the interface between the ice and quasi-liquid layer) at $T_w = 295\,K$, $H = 40$ Å, $\epsilon_{Ag-O} = 0.0611\,eV$ and $\sigma_{Ag-O} = 2.8589$ Å. Curves and scatter points are fitting and simulation results, respectively.

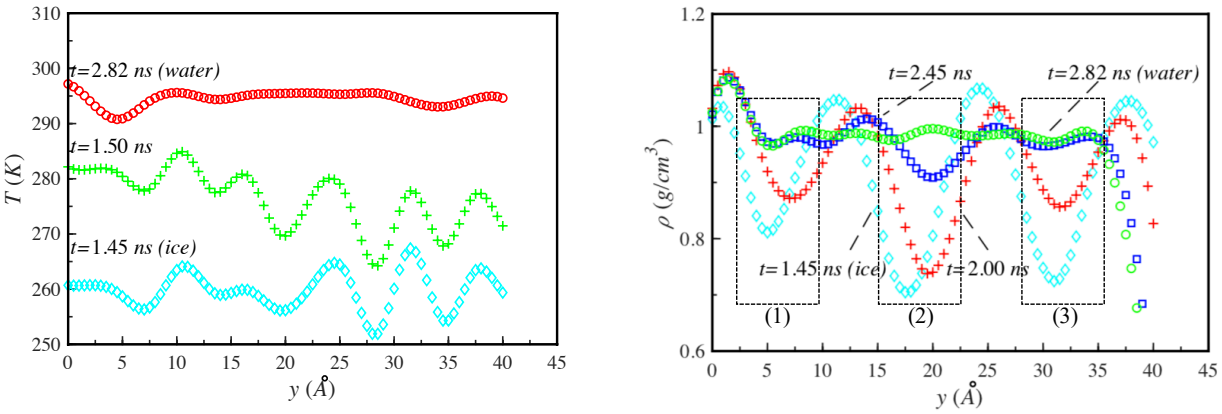

(a) (b)

Figure 8: (a) and (b): Ice/water temperature and density profiles during the thermal de-icing process at $T_w = 295\,K$, $H = 40$ Å, $\epsilon_{Ag-O} = 0.0611\,eV$ and $\sigma_{Ag-O} = 2.8589$ Å.

to each other, and are higher than the temperature for middle ice bins, which is, obviously against the simulation results shown in Fig. 8a. Particularly, the temperature decreases with fluctuations along the y direction when melting ice (i.e., $t = 1.50\,ns$), which indicates the heat flux flows from the bottom of ice to the top.

Based on the explanation of Weber et al. [44], the de-icing process from the ice mantle to the core is caused by the ice structure. Ice molecules in the bulk are firmly fixed at their corresponding locations by a strongly directional tetrad of hydrogen bonds. However, the outermost ice molecules do not have enough hydrogen bonds, and then they move inwards to form extra hydrogen bonds, which will cause extra strains and disruption of the initial network of the ice hydrogen bonds. Also, a tetrahedral entropy per molecule defined by Kumar et al.

[27] was found to be strongly related to the number of hydrogen bonds of ice/water molecules [29], and we will address the observed melting process from the view of the entropy in our future work.

The density of ice/water is displayed in Fig. 8b. The ice density profile shows regular oscillation resembling the result reported in previous investigations [18, 26]. When the melting occurs gradually, the density of ice/water then gradually decays to a steady value of $0.987\,g/cm^3$, this is in excellent agreement with the reference value of $0.997\,g/cm^3$. An interesting observation is that the local density for the top or bottom ice (see (1) and (3) marked in Fig. 8b) increases much faster than that of the middle of ice (see (2)). For example, local density for bin (1) or (3) is almost equal to the density of water while the density for the bin (2) is obviously less than the water density at $t = 2.45\,ns$. This is a piece of direct evidence that the melting process begins from the ice mantle and then proceeds inwards. Meanwhile, one can also observe that the bulk density of ice is less than that of the water, which is due to the ice crystal structure stabilized by hydrogen bonds.

5. Conclusions

We have investigated the thermal de-icing problem on a flat wall by performing molecular dynamic simulations, where the effects of the thickness of ice layer (H), wall temperature (T_w) and wettability on the melting time and the energy consumption are explored.

The results show that the melting time can be approximated as $t\,(T_w, H) = (0.9033H - 7.903)/(T_w - 273.15) + 0.01158H - 0.4005$, illustrating a linear function with respect to H and $1/(T_w - 273.15)$. The energy cost can be modelled as a linear function of the wall temperature with the slope increasing with the ice thickness: $E(T_w, H) = (0.25H + 2.078)T_w - 53.86H - 543.9$. Compared with previous studies, we revealed for the first time that the ice accumulated on a hydrophobic surface requires more time to melt compared with the hydrophilic wall, whilst the energy cost during the thermal de-icing process is independent of the wettability of the wall surface.

Through analyzing the averaged number of hydrogen bonds and the tetrahedral order parameter for each ice/water molecule, the thermal de-icing process can be roughly divided into two steps: (1) the ice temperature jumps to around the prescribed wall temperature as heat flux flows from the wall to the ice over a very short time. (2) The melting then occurs from the mantle of ice, and proceeds inwards. This work provides the insight of the physical process of thermal de-icing and guidance to the design of de-icing systems for aircraft, roads, etc.

Conflicts of interest

There are no conflicts of interest to declare.

Acknowledgements

We gratefully acknowledge the financial support from China Scholarship Council (CSC). This project has received funding from the European Union's Horizon 2020 research and innovation programme under the Marie Skłodowska-Curie grant agreement No 777717.

Appendix A. The generation of hexagonal ice crystal structure

The structure of ice I_h should follow the so-called "ice rules" [46]: there are two hydrogen atoms for each oxygen atom as the first neighbours; (2) each oxygen atom has two hydrogen atoms as the second neighbours; (3) there is only one hydrogen atom in the line joining two oxygen atoms. The pseudorandom ice configurations are generally generated based on Cota and Hoover's method [47] which is further developed in reference [48]. A new straightforward method will be employed in this work to generate the ice I_h model. An ice I_h crystal should be download from the American Mineralogist Crystal Structure Database (AMCSD), and the ice model proposed in reference [46] is used. The hexagonal crystal system of ice crystal orientation as shown in Fig. 2 (a) should be rotated to the orthogonal crystal system via the Atomsk software. Then, the prescribed ice molecules can be built through expanding the ice crystal unit by the CrystalMarker or VESTA software. Finally, the input data file for LAMMPS is generated by the VMD software.

References

[1] M. S. Kim, D.-U. Jang, J.-S. Hong, T. Kim, Thermal modeling of railroad with installed snow melting system, Cold Regions Science and Technology 109 (2015) 18–27.

[2] A. Mauro, J. C. Grossman, Street-heat: Controlling road temperature via low enthalpy geothermal energy, Applied Thermal Engineering 110 (2017) 1653–1658.

[3] T. Yongqiang, Z. Zhang, C. Jinsheng, Y. Leilei, K. Lei, Experimental study of an anti-icing method over an airfoil based on pulsed dielectric barrier discharge plasma, Chinese Journal of Aeronautics 31 (7) (2018) 1449–1460.

[4] Z. A. Janjua, B. Turnbull, S. Hibberd, K.-S. Choi, Mixed ice accretion on aircraft wings, Physics of Fluids 30 (2) (2018) 027101.

[5] M. B. Bragg, A. P. Broeren, L. A. Blumenthal, Iced-airfoil aerodynamics, Progress in Aerospace Sciences 41 (5) (2005) 323–362.

[6] R. Menini, M. Farzaneh, Advanced icephobic coatings, Journal of adhesion science and technology 25 (9) (2011) 971–992.

[7] Y. Sun, S. Wu, Q. Liu, J. Hu, Y. Yuan, Q. Ye, Snow and ice melting properties of self-healing asphalt mixtures with induction heating and microwave heating, Applied Thermal Engineering 129 (2018) 871–883.

[8] M. Chen, S. Wu, H. Wang, J. Zhang, Study of ice and snow melting process on conductive asphalt solar collector, Solar Energy Materials and Solar Cells 95 (12) (2011) 3241–3250.

[9] H. Li, Q. Zhang, H. Xiao, Self-deicing road system with a cnfp high-efficiency thermal source and mwcnt/cement-based high-thermal conductive composites, Cold Regions Science and Technology 86 (2013) 22–35.

[10] K. Liu, S. Huang, H. Xie, F. Wang, Multi-objective optimization of the design and operation for snow-melting pavement with electric heating pipes, Applied Thermal Engineering 122 (2017) 359–367.

[11] Y. Liu, H. Hu, An experimental investigation on the unsteady heat transfer process over an ice accreting airfoil surface, International Journal of Heat and Mass Transfer 122 (2018) 707–718.

[12] N. Karim, M. Zhang, S. Afroj, V. Koncherry, P. Potluri, K. S. Novoselov, Graphene-based surface heater for de-icing applications, RSC advances 8 (30) (2018) 16815–16823.

[13] J. S. Kim, A. Yethiraj, The effect of salt on the melting of ice: a molecular dynamics simulation study, The Journal of Chemical Physics 129 (12) (2008) 124504.

[14] K. Mochizuki, M. Matsumoto, I. Ohmine, Defect pair separation as the controlling step in homogeneous ice melting, Nature 498 (7454) (2013) 350–354.

[15] D. Donadio, P. Raiteri, M. Parrinello, Topological defects and bulk melting of hexagonal ice, The Journal of Physical Chemistry B 109 (12) (2005) 5421–5424.

[16] C. Ji, Y. Yan, A molecular dynamics simulation of liquid–vapour–solid system near triple-phase contact line of flow boiling in a microchannel, Applied thermal engineering 28 (2-3) (2008) 195–202.

[17] S. Engemann, H. Reichert, H. Dosch, J. Bilgram, V. Honkimäki, A. Snigirev, Interfacial melting of ice in contact with sio 2, Physical review letters 92 (20) (2004) 205701.

[18] M. A. Sánchez, T. Kling, T. Ishiyama, M.-J. van Zadel, P. J. Bisson, M. Mezger, M. N. Jochum, J. D. Cyran, W. J. Smit, H. J. Bakker, et al., Experimental and theoretical evidence for bilayer-by-bilayer surface melting of crystalline ice, Proceedings of the National Academy of Sciences 114 (2) (2017) 227–232.

[19] E. Małolepsza, T. Keyes, Water freezing and ice melting, Journal of chemical theory and computation 11 (12) (2015) 5613–5623.

[20] D. Pan, L.-M. Liu, B. Slater, A. Michaelides, E. Wang, Melting the ice: on the relation between melting temperature and size for nanoscale ice crystals, ACS nano 5 (6) (2011) 4562–4569.

[21] A. V. Egorov, E. N. Brodskaya, A. Laaksonen, Solid-liquid phase transition in small water clusters: a molecular dynamics simulation study, Molecular Physics 100 (7) (2002) 941–951.

[22] N. Nayebpanah, Fault tolerant control for bimodal piecewise affine systems (2010).

[23] E. B. Moore, E. De La Llave, K. Welke, D. A. Scherlis, V. Molinero, Freezing, melting and structure of ice in a hydrophilic nanopore, Physical Chemistry Chemical Physics 12 (16) (2010) 4124–4134.

[24] P. Rein ten Wolde, M. J. Ruiz-Montero, D. Frenkel, Numerical calculation of the rate of crystal nucleation in a lennard-jones system at moderate undercooling, The Journal of chemical physics 104 (24) (1996) 9932–9947.

[25] J. R. Errington, P. G. Debenedetti, Relationship between structural order and the anomalies of liquid water, Nature 409 (6818) (2001) 318–321.

[26] M. Conde, C. Vega, A. Patrykiejew, The thickness of a liquid layer on the free surface of ice as obtained from computer simulation, The Journal of chemical physics 129 (1) (2008) 014702.

[27] P. Kumar, S. V. Buldyrev, H. E. Stanley, A tetrahedral entropy for water, Proceedings of the National Academy of Sciences 106 (52) (2009) 22130–22134.

[28] F. Martelli, H.-Y. Ko, E. C. Oğuz, R. Car, Local-order metric for condensed-phase environments, Physical Review B 97 (6) (2018) 064105.

[29] E. Guardia, I. Skarmoutsos, M. Masia, Hydrogen bonding and related properties in liquid water: A car–parrinello molecular dynamics simulation study, The Journal of Physical Chemistry B 119 (29) (2015) 8926–8938.

[30] W. L. Jorgensen, J. D. Madura, Temperature and size dependence for monte carlo simulations of tip4p water, Molecular Physics 56 (6) (1985) 1381–1392.

[31] M. Carignano, P. Shepson, I. Szleifer*, Molecular dynamics simulations of ice growth from supercooled water, Molecular Physics 103 (21-23) (2005) 2957–2967.

[32] F. W. Starr, J. K. Nielsen, H. E. Stanley, Fast and slow dynamics of hydrogen bonds in liquid water, Physical Review Letters 82 (11) (1999) 2294.

[33] R. Kumar, J. Schmidt, J. Skinner, Hydrogen bonding definitions and dynamics in liquid water, The Journal of chemical physics 126 (20) (2007) 05B611.

[34] Y. Mao, Y. Zhang, Molecular dynamics simulation on rapid boiling of water on a hot copper plate, Applied Thermal Engineering 62 (2) (2014) 607–612.

[35] J. Abascal, E. Sanz, R. García Fernández, C. Vega, A potential model for the study of ices and amorphous water: Tip4p/ice, The Journal of chemical physics 122 (23) (2005) 234511.

[36] H. C. Andersen, Rattle: A "velocity" version of the shake algorithm for molecular dynamics calculations, Journal of Computational Physics 52 (1) (1983) 24–34.

[37] J. E. Jones, On the determination of molecular fields.—ii. from the equation of state of a gas, Proc. R. Soc. Lond. A 106 (738) (1924) 463–477.

[38] M. Papanikolaou, Molecular dynamics simulations of confined liquids in nanochannels with rough walls (2017).

[39] H. Lorentz, Ueber die anwendung des satzes vom virial in der kinetischen theorie der gase, Annalen der physik 248 (1) (1881) 127–136.

[40] D. C. R. Berthelot, No title, Hebd. Seanc. Acad. Sci. 126 (1) (1898) 1703.

[41] H. Wang, J. Zhao, Z. Chen, Experimental investigation of ice and snow melting process on pavement utilizing geothermal tail water, Energy Conversion and Management 49 (6) (2008) 1538–1546.

[42] S. Xiao, B. H. Skallerud, F. Wang, Z. Zhang, J. He, Enabling sequential rupture for lowering atomistic ice adhesion, Nanoscale 11 (35) (2019) 16262–16269.

[43] L. Bao, Z. Huang, N. V. Priezjev, S. Chen, K. Luo, H. Hu, A significant reduction of ice adhesion on nanostructured surfaces that consist of an array of single-walled carbon nanotubes: A molecular dynamics simulation study, Applied Surface Science 437 (2018) 202–208.

[44] T. A. Weber, F. H. Stillinger, Molecular dynamics study of ice crystallite melting, The Journal of Physical Chemistry 87 (21) (1983) 4277–4281.

[45] G.-J. Kroes, Surface melting of the (0001) face of tip4p ice, Surface Science 275 (3) (1992) 365–382.

[46] J. D. Bernal, R. H. Fowler, A theory of water and ionic solution, with particular reference to hydrogen and hydroxyl ions, The Journal of Chemical Physics 1 (8) (1933) 515–548.

[47] E. Cota, W. G. Hoover, Computer simulation of hexagonal ice, The Journal of Chemical Physics 67 (8) (1977) 3839–3840.

[48] J. Hayward, J. Reimers, Unit cells for the simulation of hexagonal ice, The Journal of chemical physics 106 (4) (1997) 1518–1529.